

Strange Metals from Melting Correlated Insulators in Twisted Bilayer Graphene

Peter Cha,¹ Aavishkar A. Patel,² and Eun-Ah Kim¹

¹*Department of Physics, Cornell University, Ithaca, New York 14853, USA*

²*Department of Physics, University of California, Berkeley, CA 94720, USA*

Even as the understanding of the mechanism behind correlated insulating states in magic-angle twisted bilayer graphene converges towards various kinds of spontaneous symmetry breaking, the metallic “normal state” above the insulating transition temperature remains mysterious, with its excessively high entropy and linear-in-temperature resistivity. In this work, we focus on the effects of fluctuations of the order-parameters describing correlated insulating states at integer fillings of the low-energy flat bands on charge transport. Motivated by the observation of heterogeneity in the order-parameter landscape at zero magnetic field in certain samples, we conjecture the existence of frustrating extended range interactions in an effective Ising model of the order-parameters on a triangular lattice. The competition between short-distance ferromagnetic interactions and frustrating extended range antiferromagnetic interactions leads to an emergent length scale that forms stripe-like mesoscale domains above the ordering transition. The gapless fluctuations of these heterogeneous configurations are found to be responsible for the linear-in-temperature resistivity as well as the enhanced low temperature entropy. Our insights link experimentally observed linear-in-temperature resistivity and enhanced entropy to the strength of frustration, or equivalently, to the emergence of mesoscopic length scales characterizing order-parameter domains.

Introduction - With rapid experimental developments on magic-angle twisted bilayer graphene (MATBG) reporting spin, valley, and Chern-number polarization at various integer fillings of the low-energy flat bands [1–5], a new understanding is emerging that the correlated insulating states at integer fillings [4–6] actually arise from isospin-polarization (ISP) of gapped Dirac fermions [7]. On the other hand, experiments have also found that, upon heating, these insulators with ISP melt into a “normal” state with resistivity linear in temperature T [8–11] (Fig. 1a). Further deepening the mystery is the presence of a large entropy at temperatures above the insulating transition, which is strongly enhanced non-linearly at low temperatures and rapidly quenched by an applied in-plane magnetic field (Fig. 4a). Despite much theoretical progress on understanding the nature of correlated insulators with ISP in MATBG [12–17], insight into how these experimentally observed features in the normal state arises from ISP with gapped Dirac physics remains lacking.

“Strange metal” behavior, with T -linear resistivity, is observed in many strongly correlated materials [18–20] and has long remained mysterious, as such temperature dependence is inaccessible from the limit of weakly interacting quasiparticles [21]. Recent studies of models with T -linear resistivity has shed much light on this phenomenon [22–33]. A comparative study of solvable models with local self-energy [34] identified at least two distinct mechanisms towards T -linear resistivity at temperatures below the interaction in the “incoherent” limit of perturbative electron hopping: a Mott-like mechanism where electronic transitions are confined to narrow bands separated by interaction scales, and a Sachdev-Ye-Kitaev-like mechanism where the electrons are quantum critical and the T -scaling of resistivity is a function of critical exponents. A study of a modified Hubbard model with perturbative hopping, where the ground-state de-

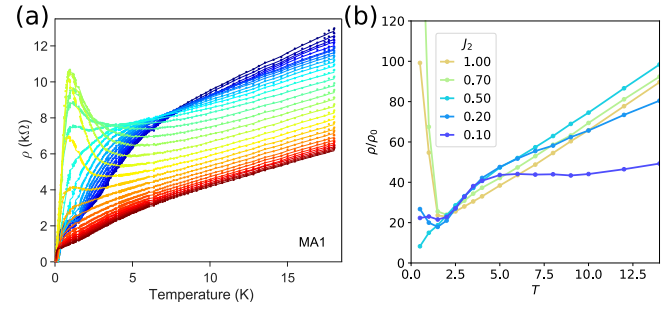


FIG. 1. (a) DC resistivity of MATBG for various fillings from $\nu = -2.4$ (blue) to $\nu = -1.5$ (red). Plot adapted from Ref. [9]. (b) DC resistivity of the Ising effective model (3) for various values of frustrating extended-range interaction J_2 . The vertical axis is in units of $\rho_0 = \hbar/(ev_D^m)^2$, where v_D^m is the effective Dirac velocity. In both (a) and (b), the progression of colors from yellow to blue indicates the lowering of the tendency to order into an insulating state at low T , although the parameters tuned are different.

generacy was broken by an extended-range interaction [25, 31], also reported T -linear resistivity. These recent advancements in understanding T -linear resistivity provide an ideal setting from which strange metal behavior in MATBG can be studied.

In this work, we capture the anticipated role of fluctuations of mesoscale domains of correlated insulator order-parameters containing ISP [3] by modeling these fluctuations within an effective Ising model with frustration. The fluctuations affect transport through coupling to the itinerant fermions. Inspired by the observations of the “Dirac revival” [35], we treat the itinerant fermions as Dirac fermions locally gapped by the order-parameters [35]. As the Dirac velocity of the flat bands is expected to be small, we treat hopping perturbatively, and model fluctuations in local ordering and ISP tendencies using

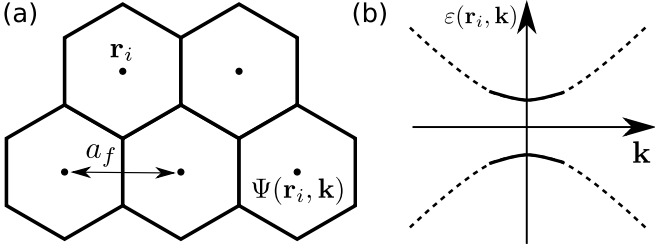


FIG. 2. (a) We coarse-grain our system into hexagonal regions \mathbf{r}_i of size a_f that form a triangular lattice. In the mean-field model (2), the Ising order-parameter $\mathcal{O}(\mathbf{r}_i)$ takes values ± 1 on each hexagonal plaquette. (b) Spectrum $\varepsilon(\mathbf{r}_i, \mathbf{k})$ near the Dirac points that have been gapped by interaction-induced symmetry breaking. Higher momentum electrons $\Psi(\mathbf{r}_i, \mathbf{k})$ in these regions are integrated out, leaving a mean field model for the modes near $\mathbf{k} = 0$.

classical Monte Carlo simulations. We then calculate the temperature dependence of the resistivity and entropy and compare our findings with recent observations.

Model - At integer fillings, we capture the effect of the insulating order-parameters with ISP at the mean-field level as a gap-inducing potential imposed on a Dirac system, *i.e.* a mass term, which may generically arise from integrating out long-range Coulomb interactions [12–17]. Such mass terms can have complicated momentum dependencies in the Brillouin zone [17]. However, in this work, we will keep the form of the mass terms as simple as possible and write the mass as $V(\mathbf{r}) = \Psi^\dagger(\mathbf{r})M\Psi(\mathbf{r})$. At charge neutrality, $\nu = 0$, $\Psi_{\sigma\tau\eta s}(\mathbf{r})$ is a 16-component spinor at spatial coordinate \mathbf{r} and σ indexes the A/B sublattices, τ denotes the graphene valley (\mathbf{K} or \mathbf{K}'), η indexes the two mini Dirac cones of MATBG [36] in a valley, and s denotes spin, and

$$M = \sum_{\alpha, \beta, \gamma, \delta=0}^3 C_{\alpha\beta\gamma\delta} \sigma^\alpha \otimes \tau^\beta \otimes \eta^\gamma \otimes s^\delta, \quad (1)$$

is a 16×16 matrix with eigenvalues ± 1 . At integer fillings away from $\nu = 0$, the ground state will be isospin-polarized and Ψ and M will have fewer components [37]. The mean-field order-parameter $\mathcal{O}(\mathbf{r}) = \langle V(\mathbf{r}) \rangle$ can then take on the normalized values ± 1 , corresponding to the different degenerate mean field ground states [38].

We will then consider the effects of long wavelength fluctuations of $\mathcal{O}(\mathbf{r})$. To do so, we divide the system into regions centered at \mathbf{r}_i , which are separated by a length scale $a_f \gg a_m$, where a_m is the moiré lattice constant of MATBG (Fig. 2a). Within each region, we then integrate out the higher momentum electron modes to obtain an effective Hamiltonian for the $\mathcal{O}(\mathbf{r}_i)$ (Fig. 2b). This is simply given by an Ising model of the $\mathcal{O}(\mathbf{r}_i)$, with longer than nearest-neighbor range interactions, which are in general allowed in an effective theory in which high energy electronic modes are integrated out [39]:

$$H_I = \sum_{i,j} U_{ij} \mathcal{O}(\mathbf{r}_i) \mathcal{O}(\mathbf{r}_j). \quad (2)$$

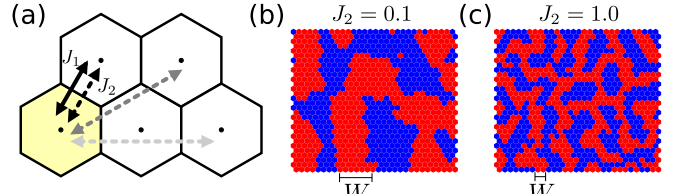


FIG. 3. (a) A visual representation of our model (3). Solid arrows denote nearest-neighbor ferromagnetic coupling J_1 , and dashed arrows denote the extended-range frustrating anti-ferromagnetic interaction J_2 , with shading indicating that the strength of the J_2 interaction falls exponentially in distance. (b, c) Configurations drawn from Monte Carlo sampling at $T = 3.5$ and $J_2 = 0.1$ (b), $J_2 = 1.0$ (c), with the emergent length scale W indicated for each configuration.

Anticipating the experimental observation of mesoscopic heterogeneity [3], we will include in U_{ij} a nearest-neighbor ferromagnetic interaction $J_1 = 1$ and an extended-range frustrating anti-ferromagnetic interaction J_2 (see Fig. 3a):

$$H_I = -J_1 \sum_{\langle ij \rangle} \mathcal{O}(\mathbf{r}_i) \mathcal{O}(\mathbf{r}_j) + J_2 \sum_{i,j} \mathcal{O}(\mathbf{r}_i) \mathcal{O}(\mathbf{r}_j) e^{-r_{ij}/l}. \quad (3)$$

Here $r_{ij} = |\mathbf{r}_i - \mathbf{r}_j|$, where \mathbf{r}_i indexes the domain sites. Although the lattice geometry of \mathbf{r}_i will not be important in our results, we work on a triangular lattice to preserve the C_3 symmetry of the Moiré sites, and take $l = 2a_f$ [40]. Given the small Dirac velocity v_D^m , we will ignore the kinetic terms from the Dirac Hamiltonian, and thus the resulting quantum fluctuations in (3). We then study the effective model of Ising variables using classical Monte Carlo.

In the low-frustration $J_2 < 1$ and intermediate-temperature $1 < T < 5$ regime, which we dub the “stripy microemulsion” regime [41], the ensemble of spatial order-parameter configurations are dominated by stripe-like mesoscale domains with an emergent length scale W . (Fig. 3b) The stripe-like appearance of the order-parameter domains in this regime follows from a mesoscopic length-scale W that satisfies $L \gg W \gg 1$, where L is the system size length scale. By contrast, away from the stripy microemulsion regime in the high-frustration $J_2 \geq 1$ or in the high-temperature $T > 5$ regimes, typical configurations are disordered with $W \sim 1$ and thus each site interacts with an effectively random distribution of Ising variables in its vicinity. (Fig. 3c) From this observed dependence of W on frustration J_2 , we conjecture a scaling form $W/a_f = F(J_2/J_1)$ where $F(x)$ is divergent for $x \leq 0$ and monotonically decreasing for $x > 0$, reaching $F(x) \sim 1$ for $x \gtrsim 1$. The emergence of W can be understood from competition between the nearest-neighbor ferromagnetic interaction J_1 , which favors long range order, with the frustrating extended range antiferromagnetic interaction J_2 , which suppresses order. The relative strength between these interactions

tunes the system between the unfrustrated Ising model, which has a divergent ordering length scale, and a frustrated, disordered system. At finite values of J_2 , we find intervening configurations featuring mesoscale domains characterized by a finite length scale W .

Transport - The low energy current operators near the mini Dirac cones take the form [42],

$$\mathbf{J}_{x,y}(\mathbf{r}) = ev_D^m \Psi^\dagger(\mathbf{r}) (\sigma^{x,y} \otimes \tau^z \otimes \eta^0 \otimes s^0) \Psi(\mathbf{r}), \quad (\nu = 0), \quad (4)$$

where e is the electron charge. In order to gap out the mini Dirac cones, the current operator must anticommute with the mass matrix M . It then follows that the action of $\mathbf{J}_x(\mathbf{r}_i)$ on the mean field ground state at \mathbf{r}_i comprising of low momentum electron modes flips $\mathcal{O}(\mathbf{r}_i) \rightarrow -\mathcal{O}(\mathbf{r}_i)$. Thus, the current operator in our effective Ising model will be $\mathbf{J}_x(\mathbf{r}_i) = ev_D^m \mathcal{X}(\mathbf{r}_i)$, where $\mathcal{X}(\mathbf{r}_i)$ is the Pauli- x operator that acts on the Ising variable of site i . We compute conductivity in the Ising effective Hamiltonian using the Kubo formula

$$\sigma(\omega) = \frac{i}{\hbar N} \sum_{n,m,i} P_n \frac{1 - e^{-\beta E_{mn}}}{E_{mn}} \frac{\langle n | \mathbf{J}_x(\mathbf{r}_i) | m \rangle \langle m | \mathbf{J}_x(\mathbf{r}_i) | n \rangle}{\omega + i\epsilon - E_{mn}}, \quad (5)$$

where N is the number of lattice sites, n and m index the ensemble of spatial order-parameter configurations, P_n is the Boltzmann factor $P_n = e^{-\beta E_n}/Z$, and $E_{mn} \equiv E_m - E_n$ are the transition energies. In the insulating states, which correspond to the low-temperature regime of our model $T < 1$, the values of $\mathcal{O}(\mathbf{r}_i)$ are frozen. Upon heating into a metallic phase, the system may then develop fluctuations of the order-parameter that will allow current to flow between the coarse-grained order-parameter domains \mathbf{r}_i .

In Fig. 1b, we plot the DC resistivity ρ_{DC}/ρ_0 against temperature T for various values of J_2 , where the unit of resistivity is $\rho_0 = \hbar/(ev_D^m)^2$. At $J_2 = 1$, which is in the high-frustration regime, we observe a slope-invariant resistivity, with no change in slope $d\rho_{DC}/dT$ from intermediate ($1 < T < 5$) to high ($T > 5$) temperatures. By contrast, at low-frustration $0 < J_2 < 1$ we observe two T -linear regimes of resistivity, at intermediate and high temperatures, with different slopes separated by a hump-like kink, indicating distinct underlying mechanisms of T -linear resistivity. Two distinct regimes of T -linear resistivity with different slopes are also seen in the experimentally measured resistivity of MATBG (Fig. 1a).

Because hopping is treated perturbatively in our model with $v_D^m \ll 1$, all of the resistivity curves presented are in the “bad metal” regime in which $\rho \gg h/e^2$. We note that the experimentally measured resistivity curve at filling $\nu = 2$ with 4 active Dirac flavors (green, Fig. 1a, see also [11]), is also largely in the bad metal regime with $\rho > h/(4e^2) = 6.45 \text{ k}\Omega$.

Insight into the slope of T -linear resistivity may be gained from an investigation of the Kubo formula (5). The second sum over states in (5) is non-vanishing only

for states m that differ from n by a sign flip at a single domain site, and thus can be written as a sum over all sites. Then the real part of conductivity can be expressed in the form

$$\frac{\sigma(\omega)}{\sigma_0} = \left\langle \left\langle \frac{1 - e^{-\beta E_{mn}}}{E_{mn}} \frac{\epsilon}{(\omega - E_{mn})^2 + \epsilon^2} \right\rangle_{m \in \text{sites}} \right\rangle_{n \sim \text{MC}}, \quad (6)$$

where $\sigma_0 = 1/\rho_0$, the inner average is taken over all sites, and the outer average is taken over MC-generated configurations which follows the Boltzmann distribution. Thus after taking the limit $\epsilon \rightarrow 0$ in Eq. (5), we may write the conductivity as

$$\frac{\sigma(\omega)}{\sigma_0} = \frac{1 - e^{-\beta \omega}}{\omega} C(\omega), \quad (7)$$

where $C(\omega) = \frac{1}{N} \sum_{n \sim \text{MC}} \sum_{m \in \text{sites}} \delta(\omega - E_{mn})$ is the spin-flip correlation function, satisfying $\int d\omega C(\omega) = 1$. The DC conductivity can then be written in the simple form $\sigma_{DC}/\sigma_0 = \beta C(0)$, from which we may conclude that T -linear resistivity is associated with a plateau of $C(0)$ in temperature. Remarkably, $C(0)$ holds simultaneous significance as the slope of T -linear resistivity and the MC- and site-averaged probability of an energy conserving, or soft, spin flip.

In the stripy microemulsion regime, soft spin flips may only take place on the boundaries of the stripe-like domains, representing fluctuations of domains that preserve W . Thus the soft spin flips that contribute towards $C(0)$ are the quasi-Goldstone gapless mode associated with the spontaneous translational symmetry breaking induced by the stripe-like heterogeneity. The spectral peak of this mode is independent of T at intermediate temperature $1 < T < 5$. This T -independent value of $C(0)$ then sets the slope of the intermediate temperature T -linear resistivity seen in Fig. 1b. This mechanism is in contrast with the T -linear resistivity away from the stripy microemulsion regime, in which each Ising site fluctuates in the vicinity of an effectively random, T -independent distribution of Ising variables. The J_2 independence of the slope of resistivity in the stripy microemulsion regime is more surprising, and can be understood as a feature of the crossover between the low frustration regime, in which the local Ising interaction is still dominant, and high-frustration regime, which is dominated by the extended-range frustration.

Entropy - Experimental investigations of integer-filled MATBG report enhanced entropy at low temperature with a non-linear dependence on temperature [43] (See Fig. 4a). We calculate entropy in the effective Ising model (2) using the formula [44]

$$S(\beta) = S(\beta = 0) + \beta \langle E \rangle - \int_0^\beta \langle E \rangle d\beta. \quad (8)$$

In Fig. 4b, we have plotted entropy vs T for a range of frustration J_2 . We observe that increasing values of J_2

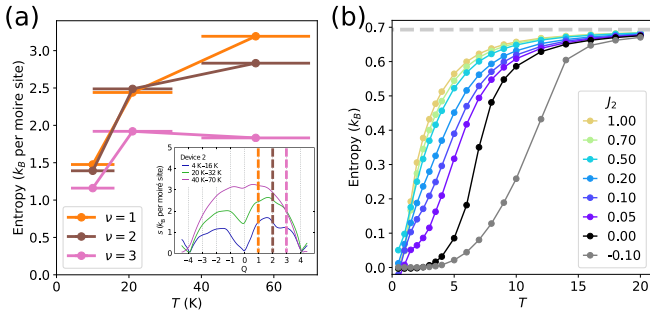


FIG. 4. (a) Entropy vs temperature T at various integer fillings of MATBG adapted from Ref. [43]. Inset: Original figure presented in Ref. [43], with vertical cuts illustrating how the data was adapted for the main figure. (b) Entropy vs temperature for various values of J_2 in our model (3). Dashed line at the value of $S = \ln 2$ indicates the extrapolated zero-temperature residual entropy.

has the effect of enhancing entropy in the low temperature regime. The concave shape of the entropy curve at intermediate temperature $1 < T < 5$ echoes the experimental results. This enhanced entropy is readily understood within the picture of mesoscale domain formation. The stripe-like domains characterized by a finite length scale W that dominate in the stripy microemulsion regime stand in sharp contrast to the unique ground state of the unfrustrated Ising model with its divergent length scale. The number of thermally accessible equivalent stripe-like configurations is extrinsic, leading to the dramatic enhancement of entropy at low temperature.

Finally, we comment on the experimentally observed sensitivity of transport and the entropy to external magnetic fields [7, 43] observed at fillings $\nu = \pm 1, \pm 2, \pm 3$. At these fillings, since the ground states are spin polarized [12, 13, 17], the spin polarization could also fluctuate like $\mathcal{O}(\mathbf{r}_i)$. Our Ising model (2) may therefore indirectly couple to the Zeeman field in a model with $SU(2)$ spin:

$$H_{I,S} = \sum_{i,j} (U_{ij}^0 + U_{ij}^1 S^z(\mathbf{r}_i) S^z(\mathbf{r}_i)) \mathcal{O}(\mathbf{r}_i) \mathcal{O}(\mathbf{r}_j) + \sum_{ij} U_{ij}^S S^z(\mathbf{r}_i) S^z(\mathbf{r}_i) + h \sum_i S^z(\mathbf{r}_i), \quad (9)$$

where h is the Zeeman field. In this spin-Ising coupled model, the entropy will be a sum of contributions from fluctuations in the Ising variable $\mathcal{O}(\mathbf{r}_i)$, captured by the effective Ising model (2), and fluctuations in spin S_z . At low temperatures, when the order-parameter sector is susceptible to mesoscale domain formation, the spin sector will also be highly susceptible to ordering. An externally applied in-plane magnetic field will then rapidly quench the entropy in the spin sector while leaving the entropy in the order-parameter sector. We speculate that such a mechanism may be responsible for the in-plane magnetic field dependence of entropy observed in Ref. [43] that is difficult to explain from a standard free Dirac fermion picture.

Discussion & conclusion - In this work, we have constructed a theory of Dirac fermions with a local mass fluctuating across space. In this theory, we have accounted for the energy cost of spatial variation in the order-parameter with an Ising variable model with nearest-neighbor ferromagnetic interaction $J_1 = 1$ as well as a extended-range frustrating anti-ferromagnetic interaction J_2 , motivated by the experimentally observed absence of long range order at zero magnetic field in some MATBG samples [3]. By an examination of the dominant order-parameter configurations, we identify a stripy microemulsion regime at low-frustration and intermediate-temperature, characterized by an emergent mesoscopic length scale W and corresponding stripe-like order-parameter domains. This length scale W arises from the competition between ferromagnetic order J_1 and frustration J_2 , and is divergent for $J_2 < 0$ and monotonically decreasing for $J_2 > 0$, reaching $W \sim 1$ in the high-frustration regime $J_2 \gtrsim 1$. In the stripy microemulsion regime, the characteristic length scale is large $L \gg W \gg 1$, and the gapless fluctuations of the stripe-like mesoscale domains are responsible for both the slope of T -linear resistivity and the enhanced entropy. Our work therefore suggests a relationship between the slope of T -linear resistivity and low-temperature entropy and the appearance of mesoscale order-parameter domains in integer-filled MATBG.

Finally, we make a few brief comments relating our work to earlier works in T -linear resistivity. An earlier work in the context of the cuprates considered a classical model in the strong-coupling limit and perturbative hopping [25]. In this work, we have applied a similar strong-coupling perspective to MATBG that yielded much insight. In addition, although in this work we have identified $T > 5$ as a “high-temperature” limit, we note that this is distinct from the ultra-high-temperature limit considered in previous studies of T -linear resistivity [34, 45], in which T is the largest scale in the problem and the thermal ensemble $e^{-\beta H}$ is proportional to the identity. Due to the extended-range of the frustrating interaction, transition energies in (5) can be as large as 20.

Interesting directions for future work remain. An experimentally observable feature of frustration is the appearance of mesoscale order-parameter domains, reminiscent of domains that have been imaged using a superconducting quantum interference device [3]. Our results suggest a relationship between the presence of frustration, the size of such order-parameter domains, and the observation of distinct regimes of T -linear resistivity and enhanced low temperature entropy. In addition, enhanced low temperature entropy with a large zero-temperature residual entropy is also observed in gapless quantum critical models [46], and may indicate the presence of a quantum critical point controlled by frustration in a quantum generalization of our effective Ising model (2), that also allows for quantum fluctuations of the order-parameter. This can be achieved by incorporating Dirac fermion modes away from zero momentum in our effective Ising

Hamiltonian, which will lead to terms coupling to transverse fields. In this quantum Ising model, we may investigate the possibility of a metallic quantum critical point at an appropriate strength of frustration, and study the behavior of the resistivity down to $T = 0$. This may be relevant to experimental settings where the twist angle between the graphene sheets is slightly detuned from the magic-angle and the insulating transition temperature is thereby suppressed nearly down to zero. Finally, while we have focused on the “bad metal” regime at integer fillings in this work, a different kind of T -linear resistivity, this time at low temperatures down to nearly $T = 0$,

is also observed when the system is doped away from integer fillings, with a magnitude much smaller than h/e^2 per Dirac flavor [8–11]. This T -linear resistivity also displays the phenomenon of “Planckian dissipation” [9, 11], which likely originates from a Fermi surface [32, 47, 48]. It would be interesting to explore how this regime is connected to the higher temperature “bad metal” regime considered here.

Acknowledgements - P.C. and E.-A.K. were supported by NSF award OAC-1934714. A.A.P. acknowledges support from the Miller Institute for Basic Research in Science.

[1] A. L. Sharpe, E. J. Fox, A. W. Barnard, J. Finney, K. Watanabe, T. Taniguchi, M. A. Kastner, and D. Goldhaber-Gordon, Emergent ferromagnetism near three-quarters filling in twisted bilayer graphene, *Science* **365**, 605 (2019).

[2] X. Lu, P. Stepanov, W. Yang, M. Xie, M. A. Aamir, I. Das, C. Urgell, K. Watanabe, T. Taniguchi, G. Zhang, A. Bachtold, A. H. MacDonald, and D. K. Efetov, Superconductors, orbital magnets and correlated states in magic-angle bilayer graphene, *Nature* **574**, 653 (2019).

[3] C. L. Tschirhart, M. Serlin, H. Polshyn, A. Shragai, Z. Xia, J. Zhu, Y. Zhang, K. Watanabe, T. Taniguchi, M. E. Huber, and A. F. Young, Imaging orbital ferromagnetism in a Moiré Chern insulator (2020), [arXiv:2006.08053 \[cond-mat.mes-hall\]](https://arxiv.org/abs/2006.08053).

[4] Y. Saito, J. Ge, K. Watanabe, T. Taniguchi, and A. F. Young, Independent superconductors and correlated insulators in twisted bilayer graphene, *Nature Physics* **16**, 926 (2020).

[5] K. P. Nuckolls, M. Oh, D. Wong, B. Lian, K. Watanabe, T. Taniguchi, B. A. Bernevig, and A. Yazdani, Strongly correlated Chern insulators in magic-angle twisted bilayer graphene, *Nature* **588**, 610 (2020).

[6] Y. Cao, V. Fatemi, A. Demir, S. Fang, S. L. Tomarken, J. Y. Luo, J. D. Sanchez-Yamagishi, K. Watanabe, T. Taniguchi, E. Kaxiras, R. C. Ashoori, and P. Jarillo-Herrero, Correlated insulator behaviour at half-filling in magic-angle graphene superlattices, *Nature* **556**, 80 (2018).

[7] Y. Saito, F. Yang, J. Ge, X. Liu, T. Taniguchi, K. Watanabe, J. I. A. Li, E. Berg, and A. F. Young, Isospin Pomeranchuk effect in twisted bilayer graphene, *Nature* **592**, 220 (2021).

[8] H. Polshyn, M. Yankowitz, S. Chen, Y. Zhang, K. Watanabe, T. Taniguchi, C. R. Dean, and A. F. Young, Large linear-in-temperature resistivity in twisted bilayer graphene, *Nature Physics* **15**, 1011 (2019).

[9] Y. Cao, D. Chowdhury, D. Rodan-Legrain, O. Rubies-Bigorda, K. Watanabe, T. Taniguchi, T. Senthil, and P. Jarillo-Herrero, Strange metal in magic-angle graphene with near Planckian dissipation, *Phys. Rev. Lett.* **124**, 076801 (2020).

[10] B. Ghawri, P. S. Mahapatra, S. Mandal, A. Jayaraman, M. Garg, K. Watanabe, T. Taniguchi, H. R. Krishnamurthy, M. Jain, S. Banerjee, U. Chandni, and A. Ghosh, Excess entropy and breakdown of semiclassical descrip-

tion of thermoelectricity in twisted bilayer graphene close to half filling (2020), [arXiv:2004.12356 \[cond-mat.mes-hall\]](https://arxiv.org/abs/2004.12356).

[11] J. M. Park, Y. Cao, K. Watanabe, T. Taniguchi, and P. Jarillo-Herrero, Flavour Hund’s coupling, Chern gaps and charge diffusivity in Moiré graphene, *Nature* **592**, 43 (2021).

[12] Y.-H. Zhang, D. Mao, and T. Senthil, Twisted bilayer graphene aligned with hexagonal boron nitride: Anomalous Hall effect and a lattice model, *Phys. Rev. Research* **1**, 033126 (2019).

[13] N. Bultinck, S. Chatterjee, and M. P. Zaletel, Mechanism for anomalous Hall ferromagnetism in twisted bilayer graphene, *Phys. Rev. Lett.* **124**, 166601 (2020).

[14] S. Liu, E. Khalaf, J. Y. Lee, and A. Vishwanath, Nematic topological semimetal and insulator in magic-angle bilayer graphene at charge neutrality, *Phys. Rev. Research* **3**, 013033 (2021).

[15] A. Thomson and J. Alicea, Recovery of massless Dirac fermions at charge neutrality in strongly interacting twisted bilayer graphene with disorder, *Phys. Rev. B* **103**, 125138 (2021).

[16] B. Lian, Z.-D. Song, N. Regnault, D. K. Efetov, A. Yazdani, and B. A. Bernevig, TBG IV: Exact insulator ground states and phase diagram of twisted bilayer graphene (2020), [arXiv:2009.13530 \[cond-mat.str-el\]](https://arxiv.org/abs/2009.13530).

[17] N. Bultinck, E. Khalaf, S. Liu, S. Chatterjee, A. Vishwanath, and M. P. Zaletel, Ground state and hidden symmetry of magic-angle graphene at even integer filling, *Phys. Rev. X* **10**, 031034 (2020).

[18] S. Martin, A. T. Fiory, R. M. Fleming, L. F. Schneemeyer, and J. V. Waszczak, Normal-state transport properties of $\text{Bi}_{2+x}\text{Sr}_{2-y}\text{CuO}_{6+\delta}$ crystals, *Phys. Rev. B* **41**, 846 (1990).

[19] R. A. Cooper, Y. Wang, B. Vignolle, O. J. Lipscombe, S. M. Hayden, Y. Tanabe, T. Adachi, Y. Koike, M. Nozawa, H. Takagi, C. Proust, and N. E. Hussey, Anomalous criticality in the electrical resistivity of $\text{La}_{2x}\text{Sr}_x\text{CuO}_4$, *Science* **323**, 603 (2009).

[20] J. A. N. Bruin, H. Sakai, R. S. Perry, and A. P. Mackenzie, Similarity of scattering rates in metals showing T -linear resistivity, *Science* **339**, 804 (2013).

[21] Y. Werman, S. A. Kivelson, and E. Berg, Non-quasiparticle transport and resistivity saturation: A view from the large- N limit, *npj Quantum Materials* **2** (2016).

[22] X.-Y. Song, C.-M. Jian, and L. Balents, Strongly corre-

lated metal built from Sachdev-Ye-Kitaev models, *Phys. Rev. Lett.* **119**, 216601 (2017).

[23] A. A. Patel, J. McGreevy, D. P. Arovas, and S. Sachdev, Magnetotransport in a model of a disordered strange metal, *Phys. Rev. X* **8**, 021049 (2018).

[24] D. Chowdhury, Y. Werman, E. Berg, and T. Senthil, Translationally invariant non-Fermi-liquid metals with critical Fermi surfaces: Solvable models, *Phys. Rev. X* **8**, 031024 (2018).

[25] C. H. Mousatov, I. Esterlis, and S. A. Hartnoll, Bad metallic transport in a modified Hubbard model, *Phys. Rev. Lett.* **122**, 186601 (2019).

[26] E. W. Huang, R. Sheppard, B. Moritz, and T. P. Devreux, Strange metallicity in the doped Hubbard model, *Science* **366**, 987 (2019).

[27] C. H. Mousatov, E. Berg, and S. A. Hartnoll, Theory of the strange metal $\text{Sr}_3\text{Ru}_2\text{O}_7$, *Proceedings of the National Academy of Sciences* **117**, 2852 (2020).

[28] A. A. Patel and S. Sachdev, Theory of a Planckian metal, *Phys. Rev. Lett.* **123**, 066601 (2019).

[29] P. Cha, N. Wentzell, O. Parcollet, A. Georges, and E.-A. Kim, Linear resistivity and Sachdev-Ye-Kitaev (SYK) spin liquid behavior in a quantum critical metal with spin-1/2 fermions, *Proceedings of the National Academy of Sciences* **117**, 18341 (2020), <https://www.pnas.org/content/117/31/18341.full.pdf>.

[30] H. Guo, Y. Gu, and S. Sachdev, Linear in temperature resistivity in the limit of zero temperature from the time reparameterization soft mode, *Annals of Physics* **418**, 168202 (2020).

[31] J. Mendez-Valderrama and D. Chowdhury, Bad metallic transport in geometrically frustrated models, *arXiv preprint arXiv:2101.00014* (2021).

[32] I. Esterlis, H. Guo, A. A. Patel, and S. Sachdev, Large N theory of critical Fermi surfaces, *arXiv preprint arXiv:2103.08615* (2021).

[33] P. T. Dumitrescu, N. Wentzell, A. Georges, and O. Parcollet, *Planckian metal at a doping-induced quantum critical point* (2021), *arXiv:2103.08607 [cond-mat.str-el]*.

[34] P. Cha, A. A. Patel, E. Gull, and E.-A. Kim, Slope invariant T -linear resistivity from local self-energy, *Phys. Rev. Research* **2**, 033434 (2020).

[35] U. Zondiner, A. Rozen, D. Rodan-Legrain, Y. Cao, R. Queiroz, T. Taniguchi, K. Watanabe, Y. Oreg, F. von Oppen, A. Stern, E. Berg, P. Jarillo-Herrero, and S. Ilani, Cascade of phase transitions and Dirac revivals in magic-angle graphene, *Nature* **582**, 203 (2020).

[36] R. Bistritzer and A. H. MacDonald, Moiré bands in twisted double-layer graphene, *Proceedings of the National Academy of Sciences* **108**, 12233 (2011).

[37] More precisely, at filling $\nu = \pm 2$, the ground state is allegedly spin polarized [12, 17], so we may just drop the s components. At $\nu = \pm 3$, we can then drop both the s and τ components [12, 13]. At $\nu = \pm 1$, we can write down a similar construction with 12 component spinors.

[38] Strictly speaking, such an interpretation requires $\Psi^\dagger(\mathbf{r})\Psi(\mathbf{r}) = 1$; this is valid as the chemical potential is in the middle of the active Dirac cones at integer fillings.

[39] Since M is larger than 2×2 , there is actually a trivial degeneracy in the states corresponding to a given value of $\mathcal{O}(\mathbf{r}_i)$, which cancels out in the computation of correlation functions up to an overall factor of the number of flavors.

[40] This value of l is sufficiently large to obtain a continuum of excited states of H_I in the thermodynamic limit, which leads to a finite conductivity.

[41] B. Spivak and S. A. Kivelson, Phases intermediate between a two-dimensional electron liquid and wigner crystal, *Phys. Rev. B* **70**, 155114 (2004).

[42] This form of the low-energy current operator is valid even when the bands are gapped and when the dispersion slows down at momenta away from the mini Dirac cones.

[43] A. Rozen, J. M. Park, U. Zondiner, Y. Cao, D. Rodan-Legrain, T. Taniguchi, K. Watanabe, Y. Oreg, A. Stern, E. Berg, P. Jarillo-Herrero, and S. Ilani, Entropic evidence for a Pomeranchuk effect in magic-angle graphene, *Nature* **592**, 214 (2021).

[44] K. Binder, Monte Carlo study of entropy for face-centered cubic Ising antiferromagnets, *Zeitschrift für Physik B Condensed Matter* **45**, 61 (1981).

[45] E. Perepelitsky, A. Galatas, J. Mravlje, R. Žitko, E. Khatami, B. S. Shastry, and A. Georges, Transport and optical conductivity in the hubbard model: A high-temperature expansion perspective, *Phys. Rev. B* **94**, 235115 (2016).

[46] S. Sachdev, Bekenstein-Hawking entropy and strange metals, *Phys. Rev. X* **5**, 041025 (2015).

[47] F. Wu, E. Hwang, and S. Das Sarma, Phonon-induced giant linear-in- T resistivity in magic angle twisted bilayer graphene: Ordinary strangeness and exotic superconductivity, *Phys. Rev. B* **99**, 165112 (2019).

[48] G. Sharma, I. Yudhistira, N. Chakraborty, D. Y. Ho, M. S. Fuhrer, G. Vignale, and S. Adam, Carrier transport theory for twisted bilayer graphene in the metallic regime, *arXiv preprint arXiv:2003.00018* (2020).